

## Grüneisen Gamma from Elastic Data

K. BRUGGER\* AND T. C. FRITZ

*Bell Telephone Laboratories, Murray Hill, New Jersey*

(Received 18 July 1966; revised manuscript received 27 September 1966)

The Grüneisen parameter  $\gamma$  is commonly used to describe anharmonic properties of solids. It can be determined from thermal data by  $\gamma = \alpha/\kappa c$ , where  $\alpha$ ,  $\kappa$ , and  $c$  are the thermal expansivity, compressibility, and heat capacity; or it can be approximated by means of continuum models from elastic data. A scalar parameter  $\gamma$  and tensorial  $\gamma_{jk}$ 's are expressed here in terms of second- and third-order elastic coefficients for arbitrary crystal symmetry, and the relations are specialized for isotropic, cubic, and rhombohedral materials. Curves of  $\gamma$  versus temperature for a variety of substances have been calculated on a digital computer on the basis of the nondispersive (Debye) and a dispersive (Born-von Karman) continuum model, and they are compared with curves obtained from thermal data.

## 1. INTRODUCTION

ANHARMONIC properties of solids are customarily described in terms of the Grüneisen parameter  $\gamma$ , familiar from the relation<sup>1</sup>

$$\gamma = \alpha/\kappa_T c_V = \alpha/\kappa_S c_P, \quad (1)$$

with  $\alpha$  the thermal volume expansivity,  $\kappa_T$  and  $\kappa_S$  the isothermal and isentropic compressibilities, and  $c_V$  and  $c_P$  the isochoric and isobaric heat capacities. In the quasiharmonic approximation, gamma can also be expressed<sup>1</sup> as the weighted average of generalized parameters  $\gamma_i$

$$\gamma = \sum_i \gamma_i c_i / \sum_i c_i, \quad (2)$$

where  $\gamma_i$  expresses the volume dependence of the lattice vibrational frequency for a mode  $i$ , and where  $c_i$  represents the Einstein heat capacity associated with that mode.

The comparison of experimental gamma values, determined from Eq. (1), with values computed from Eq. (2) would require, in principle, a detailed knowledge of the dispersion curves along many directions in the stressed and unstressed crystal, a wealth of information clearly beyond present means. For a number of solids, on the other hand, the sound speeds and their stress derivatives are known, and for these, Eq. (2) can be evaluated in a continuum model. Sheard<sup>2</sup> and Collins<sup>2</sup> investigated many cubic materials in the nondispersive model. Their approach is here extended to include dispersion and arbitrary crystal symmetry.

The scalar parameter  $\gamma$  and a tensorial gamma are derived in Sec. 2 in the nondispersive and a dispersive continuum model, and the general formulas are specialized for crystals with cubic and trigonal symmetry as well as for the isotropic case. Section 3 describes briefly the numerical calculations. Gamma-versus-temperature curves are computed for several substances and compared with their experimental counterparts in Sec. 4.

\* Present address: Ciba Limited, Basel, Switzerland.

<sup>1</sup> J. C. Slater, *Introduction to Chemical Physics* (McGraw-Hill Book Company, Inc., New York, 1939).

<sup>2</sup> F. W. Sheard, *Phil. Mag.* 3, 1381 (1958); J. G. Collins, *ibid.* 8, 323 (1963).

## 2. THEORY

## 2.1 General Relations

A crystal can be represented<sup>3</sup> by an array of atoms at rest at their mean positions with a potential energy  $\Phi$ , and an assembly of lattice vibrations with branch index  $p$ , wave vector  $\mathbf{q}$ , frequency  $\omega(p, \mathbf{q})/2\pi$ , and energies

$$E_{n(p, \mathbf{q})} = \left[\frac{1}{2} + n(p, \mathbf{q})\right] \hbar \omega(p, \mathbf{q}), \quad (3)$$

with  $n(p, \mathbf{q}) = 0, 1, 2, \dots$  and where  $\hbar$  is Planck's constant divided by  $2\pi$ . The partition function is

$$Z = e^{-\Phi/kT} \prod_{p\mathbf{q}} \sum_{n(p, \mathbf{q})} e^{-E_{n(p, \mathbf{q})}/kT}, \quad (4)$$

and the free energy  $F = -kT \ln Z$ , or

$$F = \Phi + \sum_{p\mathbf{q}} \left\{ \frac{1}{2} \hbar \omega(p, \mathbf{q}) + kT \ln [1 - e^{-\hbar \omega(p, \mathbf{q})/kT}] \right\}. \quad (5)$$

The components of the thermal expansivity tensor  $\alpha$  are given in the continuum theory of solids<sup>4</sup> by the temperature derivatives of the Lagrangian strains, taken at constant thermodynamic tension  $t$ :

$$\alpha_{jk} = [\partial \eta_{jk} / \partial T]_t. \quad (6)$$

In terms of the free energy

$$\alpha_{jk} = -s^T_{jkr} \left( \frac{\partial^2 F / V}{\partial T \partial \eta_{rs}} \right), \quad (7)$$

where the  $s^T$  are the isothermal elastic compliance coefficients and  $V$  is the crystal volume.

In the *quasiharmonic approximation*,<sup>5</sup> where  $\Phi$  and the  $\omega(p, \mathbf{q})$  are considered to depend on temperature only through the lattice dimensions, Eq. (7) becomes

$$\alpha_{jk} = \sum_{rs} \sum_{p\mathbf{q}} s^T_{jkr} \gamma_{rs}(p, \mathbf{q}) c(p, \mathbf{q}), \quad (8)$$

<sup>3</sup> J. M. Ziman, *Electrons and Phonons* (Clarendon Press, Oxford, England, 1962).

<sup>4</sup> R. N. Thurston, in *Physical Acoustics*, edited by W. P. Mason (Academic Press Inc., New York, 1964), Vol. 1A.

<sup>5</sup> G. Leibfried and W. Ludwig, in *Solid State Physics*, edited by F. Seitz and D. Turnbull (Academic Press Inc., New York, 1961), Vol. 12.

where also the generalized Grüneisen gammas<sup>6</sup>

$$\gamma_{rs}(\mathbf{p}, \mathbf{q}) = -\frac{1}{\omega(\mathbf{p}, \mathbf{q})} \left[ \frac{\partial \omega(\mathbf{p}, \mathbf{q})}{\partial \eta_{rs}} \right]_T, \quad (9)$$

do not depend directly on temperature.

$$c(\mathbf{p}, \mathbf{q}) = kx^2 e^x / (e^x - 1)^2, \quad (10)$$

with

$$x = \hbar \omega(\mathbf{p}, \mathbf{q}) / kT, \quad (11)$$

is the contribution of the mode  $\mathbf{p}, \mathbf{q}$  to the heat capacity of the crystal. The volume expansivity,  $\alpha = \sum_j \alpha_{jj}$ ,

becomes

$$\alpha = \kappa \sum_{\mathbf{p}\mathbf{q}} \gamma(\mathbf{p}, \mathbf{q}) c(\mathbf{p}, \mathbf{q}), \quad (12)$$

with  $\kappa$  the isothermal compressibility.

$$\gamma(\mathbf{p}, \mathbf{q}) = -\frac{V}{\omega(\mathbf{p}, \mathbf{q})} \left[ \frac{\partial \omega(\mathbf{p}, \mathbf{q})}{\partial V} \right]_T \quad (13)$$

is related to the tensorial  $\gamma_{rs}(\mathbf{p}, \mathbf{q})$  by

$$\kappa \gamma(\mathbf{p}, \mathbf{q}) = \sum_j \sum_{rs} s^T_{jjrs} \gamma_{rs}(\mathbf{p}, \mathbf{q}). \quad (14)$$

With

$$\gamma = \sum_{\mathbf{p}\mathbf{q}} \gamma(\mathbf{p}, \mathbf{q}) c(\mathbf{p}, \mathbf{q}) / \sum_{\mathbf{p}\mathbf{q}} c(\mathbf{p}, \mathbf{q}) \quad (15)$$

and  $c = \sum_{\mathbf{p}\mathbf{q}} c(\mathbf{p}, \mathbf{q})$ , Eq. (12) becomes Eq. (1) and Eq. (15) is Eq. (2). Similarly  $\gamma_{jk} = \alpha_{jk} / \kappa c$  with

$$\gamma_{jk} = \sum_{rs} \sum_{\mathbf{p}\mathbf{q}} s^T_{jkr s} \gamma_{rs}(\mathbf{p}, \mathbf{q}) / \kappa \sum_{\mathbf{p}\mathbf{q}} c(\mathbf{p}, \mathbf{q}). \quad (16)$$

This  $\gamma_{jk}$  is not to be confused with the

$$\bar{\gamma}_{jk} = \sum_{\mathbf{p}\mathbf{q}} \gamma_{jk}(\mathbf{p}, \mathbf{q}) c(\mathbf{p}, \mathbf{q}) / \sum_{\mathbf{p}\mathbf{q}} c(\mathbf{p}, \mathbf{q}) \quad (17)$$

of Collins and White.<sup>7</sup> They are related by

$$\kappa \gamma_{jk} = \sum_{rs} s^T_{jkr s} \bar{\gamma}_{rs}. \quad (18)$$

The *continuum model* is now introduced by the following assumptions<sup>3</sup>: (i) The excitation of optic modes can be neglected; i.e., the branch index  $\mathbf{p}$  takes only the values 1, 2, 3; (ii) The acoustic modes obey the Debye distribution function (per unit volume)

$$g(\mathbf{p}, \mathbf{q}) d\mathbf{q} d\Omega = (1/\pi^3) q^2 d\mathbf{q} d\Omega; \quad (19)$$

(iii) The maximum value of  $q$  along any direction equals the Debye radius

$$q_D = (6\pi^2/V_0)^{1/3} \quad (20)$$

<sup>6</sup> K. Brugger, Phys. Rev. 137, A1826 (1965).

<sup>7</sup> J. G. Collins and G. K. White, in *Progress in Low Temperature Physics*, edited by C. J. Gorter (North-Holland Publishing Company, Amsterdam, 1964), Vol. IV.

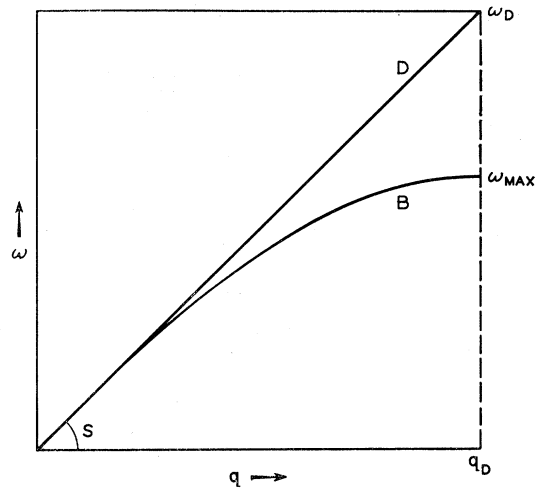


FIG. 1. Linear (Debye) and sinusoidal (Born-von Karman) dispersion relations.

[The volume of the Debye sphere equals that of the first Brillouin zone, and it is  $(2\pi)^3$  times the inverse of  $V_0$ , the volume of the primitive unit cell.]; (iv) The acoustic modes are either nondispersive (*Debye model*), or they obey the sinusoidal dispersion relation

$$\frac{\omega}{\omega_{\max}} = \sin\left(\frac{\pi q}{2 q_D}\right) \quad (21)$$

of the *Born-von Karman model*<sup>3</sup> (see Fig. 1); (v) The generalized Grüneisen parameters of Eqs. (9) and (13) are independent of wave number in both models. They are given by their long wave limits.

It should be emphasized that the choice of dispersion relations does not affect the generalized gammas but only their weight. In particular, the Born-von Karman model attributes at intermediate temperatures ( $T \sim \Theta/20$ ) a much larger weight to the low-lying branches than does the Debye model.

With these assumptions Eqs. (15) and (16) become

$$\gamma = \sum_{\mathbf{p}} \oint d\Omega \gamma(\mathbf{p}, \mathbf{N}) c(\mathbf{p}, \mathbf{N}) / \sum_{\mathbf{p}} \oint d\Omega c(\mathbf{p}, \mathbf{N}) \quad (22)$$

and

$$\gamma_{jk} = \sum_{\mathbf{p}} \oint d\Omega \sum_{rs} s^T_{jkr s} \gamma_{rs}(\mathbf{p}, \mathbf{N}) \times c(\mathbf{p}, \mathbf{N}) / \kappa \sum_{\mathbf{p}} \oint d\Omega c(\mathbf{p}, \mathbf{N}), \quad (23)$$

respectively, with

$$c(\mathbf{p}, \mathbf{N}) = \left(\frac{q_D}{2\pi}\right)^3 \int_0^1 d\xi \frac{\xi^2 Q^2 e^Q}{(e^Q - 1)^2}, \quad (24)$$

where in the Debye model

$$Q_{\text{Debye}}(\mathbf{p}, \mathbf{N}, \xi) = [\Theta(\mathbf{p}, \mathbf{N})/T] \xi \quad (25)$$

and in the Born-von Karman model

$$Q_{\text{Born}}(p, \mathbf{N}, \xi) = -\frac{2}{\pi} \frac{\Theta(p, \mathbf{N})}{T} \sin\left(\frac{\pi}{2}\xi\right). \quad (26)$$

In both,

$$\Theta(p, \mathbf{N}) = (\hbar q_D/k) S(p, \mathbf{N}) \quad (27)$$

is the characteristic temperature of the  $p$ th mode along the direction of  $\mathbf{q}$ , specified by the unit vector  $\mathbf{N}$ , and

$$S(p, \mathbf{N}) = [\partial\omega(p, \mathbf{q})/\partial q]_{q=0} \quad (28)$$

is the elastic wave speed of that mode. In terms of the  $\Theta(p, \mathbf{N})$ , the Debye temperature  $\Theta$  is given by

$$\frac{1}{\Theta^3} = \frac{1}{12\pi} \sum_p \oint \frac{d\Omega}{\Theta^3(p, \mathbf{N})}. \quad (29)$$

Expressions for the generalized gammas  $\gamma(p, \mathbf{N})$  and  $\gamma_{rs}(p, \mathbf{N})$  for these modes were given earlier<sup>6</sup> in terms of second- and third-order elastic moduli.

## 2.2 Isotropic Materials

For isotropic materials, Eq. (22) simplifies to

$$\gamma = (\gamma_l \mathcal{C}_l + 2\gamma_t \mathcal{C}_t) / (\mathcal{C}_l + 2\mathcal{C}_t), \quad (30)$$

with

$$\gamma_{l,t} = -(1/6w_{l,t}) [3B + 2w_{l,t} + k_{l,t}], \quad (31)$$

where  $B = 1/\kappa_T$  is the isothermal bulk modulus,

$$w_l = c_{11}, \quad w_t = c_{44}, \quad (32)$$

$$k_l = C_{111} + 2C_{112}, \quad k_t = \frac{1}{2}(C_{111} - C_{123}), \quad (33)$$

and in which the weighting function  $\mathcal{C}$  of Eq. (24) depends on the polarization only. The  $c$ 's are isentropic stiffnesses of the second order, and the  $C$ 's are the thermodynamically defined third-order stiffnesses determined from ultrasonic experiments.<sup>8</sup>

## 2.3 Cubic Crystals

The thermal expansion of cubic crystals is isotropic, and only the scalar  $\gamma$  of Eq. (22) is to be evaluated. For crystals with a fourfold axis the  $\gamma(p, \mathbf{N})$  are given by<sup>9</sup>

$$\gamma(p, \mathbf{N}) = -(1/6w) [3B + 2w + k], \quad (34)$$

where

$$w(p, \mathbf{N}) = c_{11}K_1 + c_{44}K_2 + c_{12}K_3, \quad (35)$$

$$k(p, \mathbf{N}) = C_1K_1 + C_2K_2 + C_3K_3, \quad (36)$$

with

$$\begin{aligned} K_1(p, \mathbf{N}) &= N_1^2 U_1^2 + N_2^2 U_2^2 + N_3^2 U_3^2, \\ K_2(p, \mathbf{N}) &= (N_2 U_3 + N_3 U_2)^2 \\ &\quad + (N_3 U_1 + N_1 U_3)^2 + (N_1 U_2 + N_2 U_1)^2, \\ K_3(p, \mathbf{N}) &= 2(N_2 N_3 U_2 U_3 + N_3 N_1 U_3 U_1 + N_1 N_2 U_1 U_2), \end{aligned} \quad (37)$$

<sup>8</sup> K. Brugger, Phys. Rev. **133**, A1611 (1964); R. N. Thurston and K. Brugger, *ibid.* **133**, A1604 (1964).

<sup>9</sup> K. Brugger, J. Appl. Phys. **36**, 767 (1965).

and

$$\begin{aligned} C_1 &= C_{111} + 2C_{112}, \\ C_2 &= C_{144} + 2C_{155}, \\ C_3 &= C_{123} + 2C_{112}. \end{aligned} \quad (38)$$

The  $N$ 's and  $U$ 's are the direction cosines for the direction of propagation and the direction of polarization characterized by the index  $p$ .

## 2.4 Rhombohedral Crystals

The thermal expansion of rhombohedral crystals is fully described by the diagonal elements of the expansivity tensor, or by  $\gamma_{\perp} = \gamma_{11} = \gamma_{22}$  and  $\gamma_{\parallel} = \gamma_{33}$ . Then also  $\gamma = 2\gamma_{\perp} + \gamma_{\parallel}$ . It is convenient to rewrite Eqs. (22) and (23) as

$$\gamma = \sum_p \oint d\Omega \Gamma(p, \mathbf{N}) \mathcal{C}(p, \mathbf{N}) / \sum_p \oint d\Omega \mathcal{C}(p, \mathbf{N}), \quad (39)$$

$$\begin{aligned} \gamma_{\perp} &= \sum_p \oint d\Omega \Gamma_{\perp}(p, \mathbf{N}) \\ &\quad \times \mathcal{C}(p, \mathbf{N}) / \sum_p \oint d\Omega \mathcal{C}(p, \mathbf{N}), \end{aligned} \quad (40)$$

$$\begin{aligned} \gamma_{\parallel} &= \sum_p \oint d\Omega \Gamma_{\parallel}(p, \mathbf{N}) \\ &\quad \times \mathcal{C}(p, \mathbf{N}) / \sum_p \oint d\Omega \mathcal{C}(p, \mathbf{N}). \end{aligned} \quad (41)$$

Here

$$\Gamma(p, \mathbf{N}) = -(B/2w) [1 + 2w\rho + r], \quad (42)$$

$$2\Gamma_{\perp}(p, \mathbf{N}) = -(B/2w) [N_1^2 + N_2^2 + 2w\rho_{\perp} + r_{\perp}], \quad (43)$$

$$\Gamma_{\parallel}(p, \mathbf{N}) = -(B/2w) [N_3^2 + 2w\rho_{\parallel} + r_{\parallel}], \quad (44)$$

where

$$\begin{aligned} w(p, \mathbf{N}) &= c_{11}R_1 + c_{66}R_2 + c_{33}R_3 \\ &\quad + c_{44}R_4 + c_{13}R_5 + c_{14}R_6, \end{aligned} \quad (45)$$

$$\begin{aligned} \rho(p) &= (s_{11} + s_{12} + s_{13})(U_1^2 + U_2^2) \\ &\quad + (2s_{13} + s_{33})U_3^2, \end{aligned} \quad (46)$$

$$\rho_{\perp}(p) = (s_{11} + s_{12})(U_1^2 + U_2^2) + 2s_{13}U_3^2, \quad (47)$$

$$\rho_{\parallel}(p) = s_{13}(U_1^2 + U_2^2) + s_{33}U_3^2, \quad (48)$$

$$r(p, \mathbf{N}) = \sum_{i=1}^6 \tau_i R_i, \quad (49)$$

$$r_{\perp}(p, \mathbf{N}) = \sum_{i=1}^6 \sigma_i R_i, \quad (50)$$

$$r_{\parallel}(p, \mathbf{N}) = \sum_{i=1}^6 \pi_i R_i, \quad (51)$$

with

$$\begin{aligned} R_1(p, \mathbf{N}) &= (N_1 U_1 + N_2 U_2)^2, \\ R_2(p, \mathbf{N}) &= (N_1 U_2 - N_2 U_1)^2, \\ R_3(p, \mathbf{N}) &= N_3^2 U_3^2, \\ R_4(p, \mathbf{N}) &= (N_2 U_3 + N_3 U_2)^2 + (N_3 U_1 + N_1 U_3)^2, \\ R_5(p, \mathbf{N}) &= 2(N_1 U_1 + N_2 U_2) N_3 U_3, \\ R_6(p, \mathbf{N}) &= 2[(N_1^2 - N_2^2) U_2 U_3 + N_2 N_3 (U_1^2 - U_2^2) \\ &\quad + 2N_1 U_1 (N_2 U_3 + N_3 U_2)]; \end{aligned} \quad (52)$$

$$\tau_i = (s_{11} + s_{12} + s_{13}) C_i' + (2s_{13} + s_{33}) C_i'', \quad (53)$$

$$\sigma_i = (s_{11} + s_{12}) C_i' + 2s_{13} C_i'', \quad (54)$$

$$\pi_i = s_{13} C_i' + s_{33} C_i'', \quad (55)$$

and

$$\begin{aligned} C_1' &= C_{111} + C_{112}, & C_1'' &= C_{113}; \\ C_2' &= \frac{1}{2}(-C_{112} + C_{222}), & C_2'' &= \frac{1}{2}(C_{113} - C_{123}); \\ C_3' &= 2C_{133}, & C_3'' &= C_{333}; \\ C_4' &= C_{144} + C_{155}, & C_4'' &= C_{344}; \\ C_5' &= C_{113} + C_{123}, & C_5'' &= C_{133}; \\ C_6' &= C_{114} + C_{124}, & C_6'' &= C_{134}. \end{aligned} \quad (56)$$

### 3. COMPUTATION

For the evaluation on a digital computer, the integrations in the previous section are transformed into summations over discrete values. For this the eigenvalue equation for elastic waves is solved for chosen directions (e.g., 45 directions or 135 modes in the half-octant for cubic crystals), and the associated solid angles, the mode gammas, the characteristic temperatures, and the Debye  $\Theta$  are calculated. After selecting a sequence of reduced temperatures, the weighting functions are obtained at each of these by numerical integration over a hundred intervals, and finally  $\gamma$  is determined at each temperature point.

### 4. RESULTS

We now proceed to calculate the gamma curves of most substances for which the necessary third-order elastic coefficients are known and whose experimental (i.e., thermal) gamma curves are available.<sup>10-54</sup> They

are listed in Table I, which also refers to the experimental data. The thermal and elastic Debye temperatures used in plotting the experimental and computed curves of  $\gamma$  versus  $T/\Theta$  are given in Table II. The thermal  $\Theta$ 's are from expansivity or heat capacity measurements and apply to zero temperature, whereas the elastic  $\Theta$ 's are calculated from room-temperature values of the elastic coefficients. Close agreement is therefore not expected. For the lack of sufficient data on the temperature dependence of the second- and, particularly, the third-order elastic coefficients and also to ease the computations, the curves were cal-

<sup>20</sup> H. J. McSkimin and P. Andreatch, J. Appl. Phys. **34**, 651 (1963).

<sup>21</sup> H. J. McSkimin and P. Andreatch, J. Appl. Phys. **35**, 2161 (1964).

<sup>22</sup> H. J. McSkimin, P. Andreatch, and R. N. Thurston, J. Appl. Phys. **36**, 1624 (1965).

<sup>23</sup> R. N. Thurston, H. J. McSkimin, and P. Andreatch, J. Appl. Phys. **37**, 267 (1966).

<sup>24</sup> D. B. Fraser and A. C. Hollis Hallett, in *Proceedings of the Seventh International Conference on Low Temperature Physics*, 1960 edited by G. M. Graham and A. C. Hollis (University of Toronto Press, Toronto, 1961).

<sup>25</sup> G. K. White, in *Proceedings of the Eighth International Conference on Low Temperature Physics*, edited by R. O. Davies (Butterworths Scientific Publications Ltd., London, 1962).

<sup>26</sup> R. J. Corruccini and J. J. Gniewek, Natl. Bur. Stds. (U.S.), Monograph **29**, (1961); R. J. Corruccini and J. J. Gniewek, *ibid.*, Monograph **21**, (1960).

<sup>27</sup> W. S. Corak *et al.*, Phys. Rev. **98**, 1699 (1955).

<sup>28</sup> J. P. Franck, F. D. Manchester, and D. L. Martin, Proc. Roy. Soc. (London) **A263**, 494 (1961).

<sup>29</sup> D. L. Martin, Can. J. Phys. **38**, 17 (1960).

<sup>30</sup> C. E. Monfort and C. A. Swenson, J. Phys. Chem. Solids **26**, 291 (1965).

<sup>31</sup> R. H. Stokes, J. Phys. Chem. Solids **27**, 51 (1966).

<sup>32</sup> S. L. Quimby and S. Siegel, Phys. Rev. **54**, 293 (1938).

<sup>33</sup> G. K. White, Proc. Roy. Soc. (London) **A286**, 204 (1963).

<sup>34</sup> D. L. Martin, Phil. Mag. **46**, 751 (1955).

<sup>35</sup> K. Clusius, J. Goldman, and A. Perlick, Z. Naturforsch. **4a**, 424 (1949).

<sup>36</sup> C. V. Briscoe and C. F. Squire, Phys. Rev. **106**, 117 (1957).

<sup>37</sup> G. K. White, J. Australian Inst. Metals **8**, 134 (1963).

<sup>38</sup> P. P. M. Meincke and G. M. Graham, Can. J. Phys. **43**, 1853 (1965).

<sup>39</sup> J. A. Morrison and D. Patterson, Trans. Faraday Soc. **52**, 764 (1956).

<sup>40</sup> W. C. Overton and R. T. Swim, Phys. Rev. **84**, 758 (1951).

<sup>41</sup> W. T. Berg and J. A. Morrison, Proc. Roy. Soc. (London) **A242**, 467 (1957).

<sup>42</sup> M. H. Norwood and C. V. Briscoe, Phys. Rev. **112**, 45 (1958).

<sup>43</sup> T. H. K. Barron, W. T. Berg, and J. A. Morrison, Proc. Roy. Soc. (London) **A250**, 70 (1959).

<sup>44</sup> R. D. McCammon and G. K. White, Phys. Rev. Letters **10**, 234 (1963).

<sup>45</sup> R. H. Carr, R. D. McCammon, and G. K. White, Phil. Mag. **12**, 157 (1965).

<sup>46</sup> P. Flubacher, A. J. Leadbetter, and J. A. Morrison, Phil. Mag. **4**, 273 (1959).

<sup>47</sup> H. J. McSkimin, J. Appl. Phys. **24**, 988 (1953).

<sup>48</sup> G. K. White, Cryogenics **4**, 2 (1964).

<sup>49</sup> R. B. Sosman, *Phases of Silica* (Rutgers University Press, New Brunswick, New Jersey, 1965).

<sup>50</sup> F. C. Nix and D. MacNair, Rev. Sci. Instr. **12**, 66 (1941).

<sup>51</sup> R. C. Lord and J. C. Morrow, J. Chem. Phys. **26**, 230 (1957).

<sup>52</sup> H. A. Leadbetter and J. A. Morrison, Phys. Chem. Glasses **4**, 188 (1963).

<sup>53</sup> P. Flubacher, A. J. Leadbetter, J. A. Morrison, and B. P. Stoicheff, J. Phys. Chem. Solids **12**, 53 (1959).

<sup>54</sup> H. J. McSkimin, cited by O. L. Anderson, in *Progress in Very High Pressure Research*, edited by F. P. Bundy *et al.* (John Wiley & Sons, Inc., New York, 1961).

<sup>10</sup> W. B. Daniels and C. S. Smith, Phys. Rev. **111**, 713 (1958).

<sup>11</sup> P. A. Smith and C. S. Smith, J. Phys. Chem. Solids **26**, 279 (1965).

<sup>12</sup> W. R. Marquardt and J. Trivisonno, J. Phys. Chem. Solids **26**, 273 (1965).

<sup>13</sup> W. B. Daniels, Phys. Rev. **119**, 1246 (1960).

<sup>14</sup> R. A. Miller and C. S. Smith, J. Phys. Chem. Solids **25**, 1279 (1964).

<sup>15</sup> R. A. Bartels and D. E. Schuele, J. Phys. Chem. Solids **26**, 537 (1965).

<sup>16</sup> L. M. Roberts, Proc. Roy. Soc. (London) **B70**, 744 (1957).

<sup>17</sup> E. H. Bogardus, J. Appl. Phys. **36**, 2504 (1965).

<sup>18</sup> G. K. White and O. L. Anderson, J. Appl. Phys. **37**, 430 (1966).

<sup>19</sup> H. J. McSkimin and P. Andreatch, J. Appl. Phys. **35**, 3312 (1964).

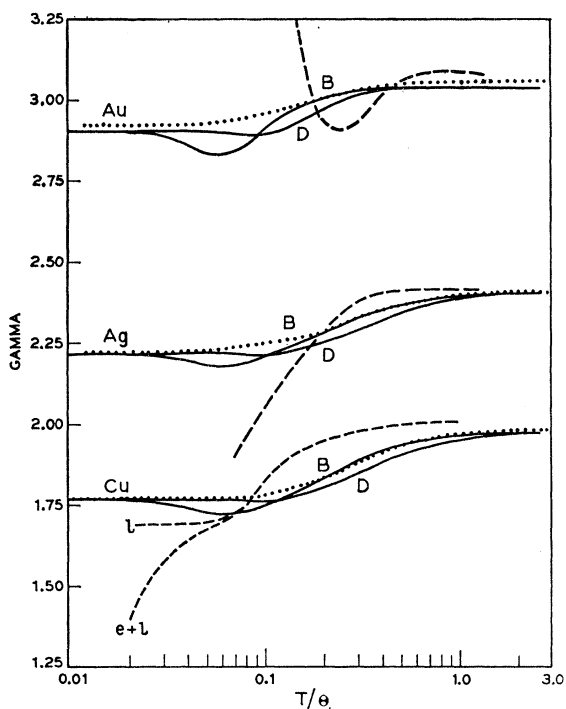


FIG. 2. Elastic (solid curve) and thermal (dashed curve)  $\gamma$ -versus- $T/\Theta$  curves for Au, Ag, and Cu.  $l$  and  $e+l$  label the  $\gamma$  curves of copper for the lattice alone, and for the electrons and the lattice, respectively. (Dotted curve) after Collins in Ref. 2.

culated from room-temperature data only. The effect of this simplification will be illustrated in Sec. 4.2 for the case of potassium chloride. In the figures the labels  $D$  and  $B$  designate the curves based on the Debye and on the Born-von Karman dispersion relations, respectively. The thermal curves are dashed. The dotted curves in Figs. 2 and 4 are representative of Collins's results<sup>2</sup> based in part on older elastic data. They differ from our computed curves mainly by a more gradual ascent between 0.1 and 1.0  $T/\theta$ , attributable to their integration procedure.

TABLE I. References.

Material	Elastic data <sup>a</sup>	Thermal data <sup>b</sup>
Au	2, 3(10)	$\alpha$ (24,26), $c$ (26)
Ag	2, 3(10)	$\alpha$ (24,25,26), $c$ (26)
Cu	2, 3(10)	$\alpha$ (7,24), $c$ (27,28,29)
K	2, 3(11), 2(12)	$\alpha$ (30,31), $c$ (30), $B$ (30)
Na	2, 3(13)	$\alpha$ (26), $c$ (26), $B$ (32)
LiF	2, 3(14)	$\alpha$ (33), $c$ (34,35), $B$ (36)
NaCl	2, 3(15)	$\alpha$ (33,37,38), $c$ (39) $B$ (17,40)
NaF	2, 3(14)	
KCl	2, 3(15), 2(16)	$\alpha$ (33,37,38), $c$ (41), $B$ (42)
MgO (cryst.)	2, 3(17)	$\alpha$ (16), $c$ (43), $B$ (16)
MgO (polycryst.)	2, 3(18)	
Ge	2, 3(19,20)	$\alpha$ (44,45), $c$ (46), $B$ (47)
Si	2, 3(19,21)	$\alpha$ (44,45), $c$ (46), $B$ (47)
$\alpha$ -SiO <sub>2</sub>	2, 3(22,23)	$\alpha$ (48,49,50), $c$ (51), $B$ (22)
Vitr. SiO <sub>2</sub>	2, 3(15)	$\alpha$ (44), $c$ (52,53), $B$ (54)

<sup>a</sup> 2 and 3 refer to second- and third-order elastic coefficients, respectively.  
<sup>b</sup>  $\alpha$ ,  $c$ , and  $B$  refer to data on expansivity, heat capacity, and the temperature dependence of the bulk modulus.

TABLE II. Debye temperatures.

Material	Debye temperature $\Theta$ (°K)	
	Elastic	Thermal
Au	155.6	180
Ag	216.1	215
Cu	330.9	315
K	77.4	89
Na	133.4	158
LiF	698.0	737
NaCl	304.6	322
NaF	475.1	...
KCl	224.3	238
MgO (cryst.)	939.3	950
MgO (polycryst.)	933.0	...
Ge	369.9	375
Si	645.5	650
$\alpha$ -SiO <sub>2</sub>	586.4	600
Vitr. SiO <sub>2</sub>	499.5	490

Continuum models allow the computation of thermodynamic properties from only a few experimental parameters, but they apply only to dielectric monatomic, primitive crystals, which have not been provided by nature. In these applications, therefore, the neglect of dispersion in the generalized gammas, of conduction electrons in metals, and of optic modes, where they occur, may become serious, shedding light on their importance in real crystals.

#### 4.1 Noble and Alkali Metals

The calculated and experimental curves for the noble metals Au, Ag, Cu and for the alkali metals K, Na are drawn in Figs. 2 and 3. Their agreement is fair except at low temperatures where the experimental gammas are affected by the conduction electrons. Separating the electronic and the lattice contributions into the expansivity and the heat capacity, Eq. (1) becomes

$$\gamma = \frac{\alpha}{\kappa c} = \frac{\alpha_e + \alpha_l}{\kappa(c_e + c_l)} \quad (57)$$

The continuum model, on the other hand, gives the

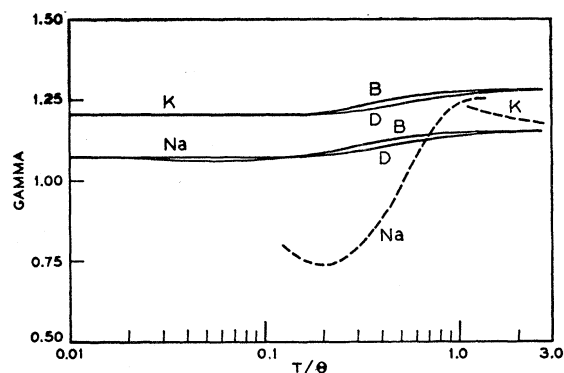


FIG. 3. Elastic (solid curve) and thermal (dashed curve)  $\gamma$ -versus- $T/\Theta$  curves for K and Na.

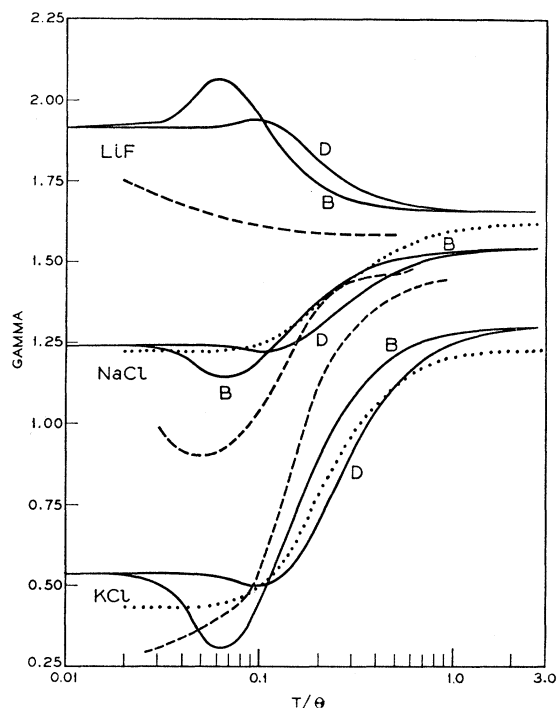


FIG. 4. Elastic (solid curve) and thermal (dashed curve)  $\gamma$ -versus- $T/\theta$  curves for LiF, NaCl, and KCl. (Dotted curve) after Collins in Ref. (2).

lattice gamma

$$\gamma_l = \alpha_l / \kappa c_l, \quad (58)$$

which one wishes to compare with the experimental gamma for the lattice alone,

$$\gamma_l = (\alpha - \alpha_e) / \kappa (c - c_e). \quad (59)$$

This was illustrated for the case of copper by Collins and White,<sup>7</sup> who measured the expansivity precisely enough and to low enough temperatures to determine  $\alpha_e$  (proportional to  $T$ ) and  $\alpha_l$  (proportional to  $T^3$ ) separately, with an electronic gamma,

$$\gamma_e = \alpha_e / \kappa c_e, \quad (60)$$

of 0.9, close to the free-electron value of  $\frac{2}{3}$ . Their curves for the lattice and for the total gamma are labeled  $l$  and  $e+l$ , respectively, in Fig. 2. For the other metals of Figs. 2 and 3, values of  $\alpha_e$  are not available, and their lattice gammas cannot be obtained separately. But it seems likely that in gold and silver the conduction electrons, rather than dispersion, cause the pronounced

TABLE III.  $\gamma_\infty - \gamma_0$  for noble metals and for alkali metals.

Material	$\gamma_\infty - \gamma_0$ (calculated)
Au	0.135
Ag	0.185
Cu	0.200
K	0.075
Na	0.080

TABLE IV. Low-gamma shear modes for NaCl-type structure.

Material	$r^-/r^+$ <sup>a</sup>	Mode <sup>b</sup> gamma	$\gamma_0 - \gamma_\infty$ (calculated)
LiF	2.27	0.53	0.26
MgO	2.18	0.42	0.11
NaCl	1.90	0.12	-0.28
NaF	1.43	-0.04	-0.31
KCl	1.36	-0.77	-0.76

<sup>a</sup> Ionic radii from *Handbook of Chemistry and Physics*, edited by C. D. Hodgeman *et al.*, (Chemical Rubber Publishing Company, Cleveland, Ohio, 1958), 40th ed.

<sup>b</sup> For  $c_{44}$  shear modes.

deviation of the thermal gamma from the computed curves for  $T/\theta < 0.2$ . For sodium, matters are complicated by the Martensitic transformation,<sup>55</sup> from the close-packed cubic to hexagonal phase, centered around  $T/\theta \sim 0.3$ .

The computed curves have the general shape predicted by Barron<sup>56</sup> from lattice calculations. The differences between high- and low-temperature limits of gamma listed in Table III conform with his theory for a fcc lattice, predicting a value of 0.3 for central nearest-neighbor forces and a decrease of this value when more distant neighbors also interact. For the bcc structure of K and Na no lattice calculations have been made.

#### 4.2 Alkali Halides and Magnesium Oxide

Figures 4 and 5 show gamma curves for LiF, NaCl, NaF, and KCl. The computations reproduce the experimental data quite well, in particular the trend in the magnitude of gamma with the anion overlap noted by White<sup>37</sup> in the analysis of his expansivity data. A decreasing overlap reduces the shear stiffnesses, particularly  $c_{44}$  (and finally the NaCl-type lattice transforms to the CsCl structure). The data of Table IV show also the generalized gammas associated with the  $c_{44}$  shear modes to decrease monotonically with decreasing ratio of anion to cation radii, a measure of this

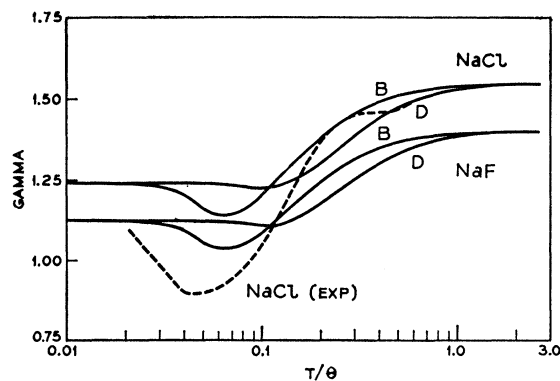


FIG. 5. Elastic (solid curve) and thermal (dashed curve)  $\gamma$ -versus- $T/\theta$  curves for NaF and NaCl.

<sup>55</sup> D. L. Martin, Proc. Roy. Soc. (London) A254, 433 (1960).

<sup>56</sup> T. H. K. Barron, Phil. Mag. 46, 720 (1955).

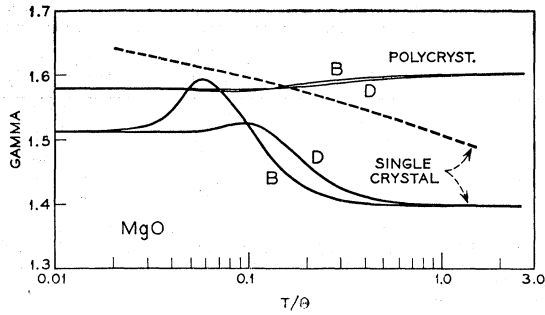


FIG. 6. Elastic (solid curve) and thermal (dashed curve)  $\gamma$ -versus- $T/\theta$  curves for polycrystalline and a single crystal of MgO.

overlap. This then lowers the parameter  $\gamma$  progressively over the whole temperature range, but particularly at low temperatures, as is illustrated in the last column of this table by the difference between the low- and high-temperature limits.

MgO, isomorphous with these alkali halides, fits the same pattern and it is included in Table IV. Gamma curves for a single crystal and a hot pressed polycrystalline specimen are shown in Fig. 6.

It has been mentioned above that only room temperature values of the elastic coefficients have been used in the computation of all these gamma curves. Such a curve labeled  $\gamma_D$  for KCl in the Debye model is repeated in Fig. 7. A second curve  $\gamma'$  results when the weight functions are computed from low-temperature data at 4.2°K<sup>16</sup> while maintaining the room-temperature generalized gammas, and a third curve  $\gamma''$  is the result of using the same low-temperature data for the weight functions but with generalized gammas now determined at an intermediate temperature (195°K)<sup>15</sup>. The low-temperature limit  $\gamma_0$  finally is estimated assuming,

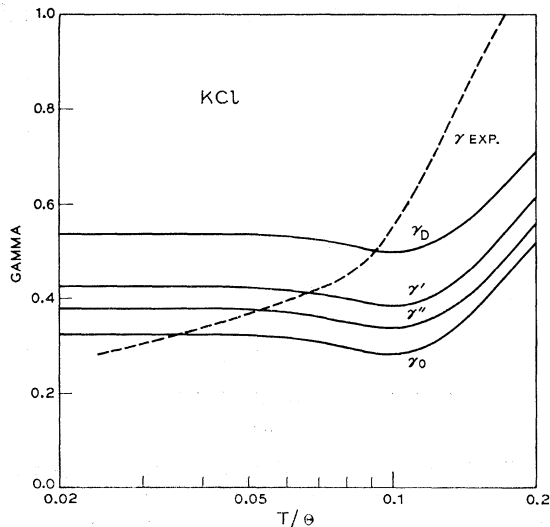


FIG. 7. Determination of  $\gamma_0$  for KCl.

after Bartels and Schuele,<sup>15</sup>  $\gamma(T)$  to be proportional to the specific volume. For KCl with its strongly temperature-dependent  $\gamma$ , this correction is quite drastic, indicating the need for measurements of third-order coefficients in the liquid-helium range.

#### 4.3 Germanium and Silicon

The thermal curves for both Ge and Si in Fig. 8 show broad minima in the low-temperature region with the thermal expansivity becoming negative over extended intervals, but climbing again toward the calculated low-temperature limits. This behavior is shared by indium antimonide<sup>57</sup> and other solids with a diamond or zinc-blende-type lattice, and has been discussed by Carr *et al.*<sup>45</sup> The relatively open structure favors low lying, highly dispersive modes,<sup>58</sup> with negative gammas near the zone edge<sup>59,60</sup> becoming dominant in the low-temperature region. Optic modes<sup>59</sup> cause the steep rise above  $T/\theta \sim 0.1$  leading the elastic and thermal gammas to agree near  $T \sim \theta$ . The dots in Fig. 8 represent Bienenstock's<sup>59</sup> calculation for Ge based on a modified shell model with an adjustable parameter and including optic modes in the Einstein approximation.

#### 4.4 $\alpha$ -Quartz and Vitreous Silica

It may be noted, first of all, that for the determination of the scalar gamma the third-order elastic coefficients are required only in those combinations which can be obtained from sound-speed measurements under hydrostatic pressure. For tensorial gammas, how-

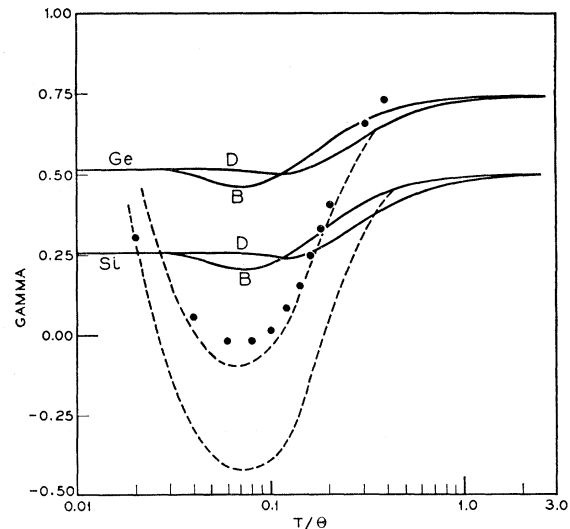


FIG. 8. Elastic (solid curve) and thermal (dashed curve)  $\gamma$ -versus- $T/\theta$  curves for Ge and Si. (●) after Bienenstock in Ref. (59) for Ge.

<sup>57</sup> D. F. Gibbons, Phys. Rev. **112**, 136 (1958).

<sup>58</sup> B. N. Brockhouse and P. K. Iyengar, Phys. Rev. **111**, 747 (1958); B. N. Brockhouse, Phys. Rev. Letters **2**, 256 (1959).

<sup>59</sup> A. Bienenstock, Phil. Mag. **9**, 755 (1964).

<sup>60</sup> R. T. Payne, Phys. Rev. Letters **13**, 53 (1964).

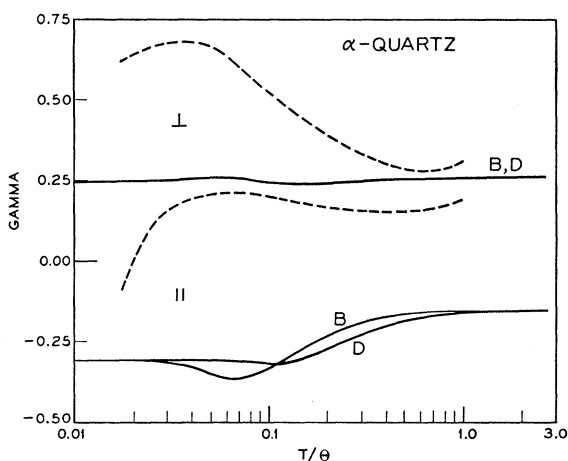


FIG. 9. Elastic (solid curve) and thermal (dashed curve)  $\gamma$ -versus- $T/\Theta$  curves for  $\alpha$ -quartz, perpendicular ( $\perp$ ) and parallel ( $\parallel$ ) to the threefold axis.

ever, uniaxial stress data are needed for all but cubic crystals.

Figure 9 depicts the gammas perpendicular ( $\perp$ ) and parallel ( $\parallel$ ) to the threefold axis of  $\alpha$ -quartz, whereas the gamma related to the volume expansivity is shown in Fig. 10 together with the curves for vitreous silica. The computed  $\gamma_I$  curve lies, correctly, above  $\gamma_{II}$ , and the latter is negative over the whole temperature range, while the experimental  $\gamma_{II}$  becomes negative only at very low temperatures ( $T < 12^\circ\text{K}$ ). The thermal gammas along both directions exhibit broad maxima centered near  $30^\circ\text{K}$ . At the upper end of the temperature range, approaching the  $\alpha$ - $\beta$  transition, gamma exhibits a further moderate increase.

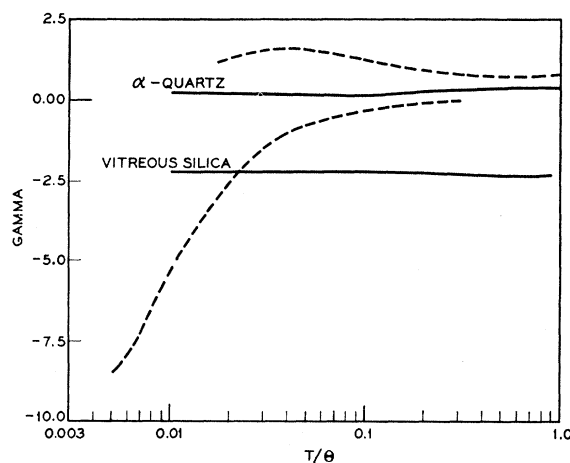


FIG. 10. Elastic (solid curve) and thermal (dashed curve)  $\gamma$ -versus- $T/\Theta$  curves for  $\alpha$ -quartz ( $\gamma = 2\gamma_I + \gamma_{II}$ ) and vitreous silica.

The lack of closer agreement between elastic and thermal curves is not surprising in view of the complicated structure of  $\alpha$ -quartz,<sup>49</sup> with nine atoms in the primitive unit cell. The broad hump at low temperatures is presumably due to optic modes. At least this assumption is not inconsistent with a small excess heat capacity.<sup>52</sup> This effect is present in vitreous silica to a much larger degree and leads to an extraordinarily large negative expansivity<sup>48</sup> at a temperature as low as  $2^\circ\text{K}$ .

#### ACKNOWLEDGMENT

With pleasure we acknowledge valuable discussions with G. K. White.